Energy Proceedings
Vol 35, 2023
ISSN 2004-2965

Dynamics Behavior and Settling Velocity Prediction of Dry Ice in Ocean Sequestration

Jieshuo ZHANG[1], Wei WEI[1,2], Mingjian LU[2,3,4,*]

1. School of Transportation and Logistics Engineering, Wuhan University of Technology, Wuhan, 430063, China

2. National Engineering Research Center for Water Transport Safety (WTs Center, MoST), Wuhan University of Technology, Wuhan 430063, China

3. Intelligent Transportation Systems Research Center, Wuhan University of Technology, Wuhan 430063, China

4. State Key Laboratory of Maritime Technology and Safety, Wuhan University of Technology,Wuhan 430063, China

([*]Corresponding Author: mingjian_lu@whut.edu.cn)

Abstract

Ocean carbon sequestration is a process of storing captured CO2 in the ocean, using liquid or solid forms of storage. Compared to liquid CO2 sequestration, dry ice ocean sequestration is simpler, more efficient, and has a larger capacity. However, research on the free-settling process of dry ice in ocean sequestration is still lacking, which limits the efficiency of dry ice ocean sequestration. In this study, the settling process of bullet-shaped dry ice is researched, and different models are established based on the main shape factors. The six-degree-of-freedom dynamic mesh is adopted to simulate the free settling of dry ice, and the mesh is kept near dry ice unchanged to ensure numerical simulation accuracy. The study shows that shapes with larger ellipticity of the front end have lower drag coefficients, and the shape factors mainly depend on ellipticity to influence the settling velocity. The correlation between Reynolds number and shape factors is obtained to predict the settling terminal velocity of bullet-shaped dry ice, providing a reference for the shape design of dry ice sequestration. This research provides theoretical support and practical guidance for efficient dry ice ocean sequestration.

Keywords: Ocean sequestration; Free settling; Settling velocity; Shape factor

NONMENCLATURE

Abbreviatdions	
CCUS	Carbon Capture, Utilization and Storage
Symbols	
C_d	Drag coefficient
C_p	Pressure coefficient
Re	Reynolds number
r_1, r_2, h	Shape parameters
k_1, k_2	Shape factors
ρ	Density
μ	Dynamic viscosity
u	Velocity
F	Resistance
S	Projected area
l_c	Characteristic length
V	Volume

1. INTRODUCTION

Carbon emission reduction methods include energy substitution, energy conservation and efficiency enhancement, and carbon capture, utilization and storage (CCUS). While green new energy technologies are promising, they face issues such as high costs and immature technology. Improving ship efficiency has limited potential to reduce carbon emissions. CCUS technology is currently one of the most effective technologies for significantly reducing carbon emissions

This is a paper for International CCUS Conference 2023 (ICCUSC2023), April 14-15, 2023, Beijing, China.

in the shipping industry[1]. Various CCUS projects for different ships have been carried out worldwide to promote the advancement of CCUS technology. For example, DNV GL collaborated with Process Systems Enterprise to develop the "Eurostar" concept design[2], which captures CO2 from ship diesel engine exhaust and stores it as a liquid for transportation through ports, achieving a carbon reduction of approximately 65%. In another project, the "decarbon ICE" project[3] proposed using low-temperature treatment technology to convert CO2 in ship exhaust into streamlined dry ice for ocean sequestration, reducing carbon emissions by 90%. Kawasaki K Line, Mitsubishi Shipbuilding Company, and the Japan Marine United Corporation are collaborating on the "Carbon Capture on the Ocean" project[4], developing a compact carbon capture device and verifying the operability and safety of the onboard carbon capture system.

Regarding the free settling of objects in fluid media, various researchers have conducted experiments and numerical simulations on different types of settling particles. Based on experimental data on the free fall of cylindrical particles, Gabitto[5] established an explicit equation for the drag coefficient and terminal velocity of freely falling cylindrical particles using the length-diameter ratio to describe particle shape. Dioguardi[6] proposed a shape factor to describe the shape of irregular particles based on experimental measurements of the final settling velocity of particles in fluids of different densities and viscosities and obtained relevant laws and correlations between drag coefficient, Reynolds number, and shape factor. Specific shapes and sizes of particles can be calculated iteratively to obtain the final velocity. Li[7] studied the experimental settling data of 320 plate fragments and found that the settling velocity of plate fragments is closely related to the nominal diameter and Corey shape factor. Based on this, they established a practical equation linking dimensionless settling velocity, dimensionless diameter, and Corey shape factor for plate-shaped particles with acceptable accuracy. Gong[8] validated two-dimensional and three-dimensional cylindrical RANS simulation flows, predicted the drag coefficient using CFD, and studied the free settling of horizontal cylinders under static water and water flow.

Unlike ordinary solids, dry ice will sublimate directly from a solid state to a gaseous state when it heats up. In 1991, Nakashiki[9] conducted experiments on the volume loss of cubic dry ice during its free settling in the ocean. Cubic dry ice with side lengths of 22.2 cm and 18.4 cm was dropped at a velocity of 0.56 m/s and completely lost at depths of 534 m and 484 m, with loss rates of 2.3×10^{-2} g/s·cm^2 and 2.1×10^{-2} g/s·cm^2, respectively. According to the CO_2 three-phase diagram, when the solid CO_2 sinks to a certain depth in the ocean, the water pressure is higher than the CO_2 triple point, and the solid dry ice no longer sublimates. Therefore, for the sinking of large-sized solid dry ice, whether it is in the sinking development stage or the deep sea, the volume loss is very small, and the sinking body of dry ice can be treated as a constant volume.

Ocean dry ice throwing is an effective method for mitigating greenhouse gas emissions in the shipping industry and can serve as a means of carbon sequestration in the ocean. However, due to experimental limitations, research on large-scale streamlined free settling is still lacking, and the sizes of experimental and numerical simulation settling bodies are limited to small-scale. In this study, the free-settling process of large-scale streamlined objects was investigated, and two dimensionless shape factors were defined to explore the influence of shape factors on dynamics behavior during free settling. An equation for predicting settling velocity through the shape factor was obtained, providing theoretical support and design reference for the marine dry ice-throwing carbon sequestration.

2. NUMERICAL METHOD AND PHYSICAL MODEL

2.1 Six DOF dynamic mesh method and validation

The six DOF dynamic mesh method uses the force and moment of the object to calculate the translational and angular motion of the object's center of gravity. The governing equations of the translational motion of the center of gravity are solved in the inertial coordinate system.

$$\overrightarrow{v_{\mathrm{G}}} = \frac{1}{m}\sum \overrightarrow{f_{\mathrm{G}}} \tag{1}$$

where $\overrightarrow{v_{\mathrm{G}}}$ is the translational acceleration of the center

of mass, m is the mass of the object, $\overrightarrow{f_G}$ is the force vector caused by gravity.

Angular acceleration $\overrightarrow{\omega_B}$ is solved in object coordinates.

$$\overrightarrow{\omega_B} = L^{-1}\left(\sum \overrightarrow{M_B} - \overrightarrow{\omega_B} \times L\overrightarrow{\omega_B}\right) \tag{2}$$

The torque experienced by the object in the inertial coordinate system is converted to the object coordinate system by the following method.

$$\overrightarrow{M_B} = R\overrightarrow{M_G} \tag{3}$$

where R is the following transformation matrix.

$$\begin{pmatrix} C_\theta C_\psi & C_\theta S_\psi & -S_\theta \\ S_\phi S_\theta C_\psi - C_\phi S_\psi & S_\phi S_\theta S_\psi + C_\phi C_\psi & S_\phi C_\theta \\ C_\phi S_\theta C_\psi + S_\phi S_\psi & C_\phi S_\theta S_\psi - S_\phi C_\psi & C_\phi C_\theta \end{pmatrix} \tag{4}$$

where $C_\chi = cos(\chi)$, $S_\chi = sin(\chi)$, and ϕ, θ, ψ are respectively Euler angles representing rotations about the x,y, and z axes.

After the angular acceleration and translational acceleration of the object are calculated by equations (1) and (2), the angular motion and translational motion velocity are obtained by numerical integration, and the position of the rigid body is further updated by dynamic mesh.

The lack of relevant research and experimental data on the settling of large-scale objects makes it difficult to validate, while there is more research on small-sized spherical particles. The C_d-Re empirical formula (Equation 5) proposed by Cheng[11] has high accuracy and applies to the subcritical range (Re<2×10^5):

$$C_d = \frac{24}{Re}\left(1+0.27Re\right)^{0.43} + 0.47\left[1-\exp(-0.04Re^{0.38})\right] \tag{5}$$

The free settling of a spherical particle with density ρ=1500 kg/m^3 and diameter d=100 mm was selected for validation. The specific validation results are shown in Table 1.

Table 1. Validation results

Terminal velocity/(m·s^{-1})	Re	$C_{d,simul}$	$C_{d,exp}$	Relative error/%
1.17	116440	0.4811	0.4715	2.05

As shown in Table 1, the terminal velocity of the free settling of numerical simulation is 1.17 m/s, the drag coefficient $C_{d,simul}$=0.4811 is calculated according to the definition of drag coefficient 1.7, and $C_{d,exp}$=0.4715 is calculated according to the empirical formula iteratively. The relative error between the two is 2.05%, thus the feasibility of numerical simulation can be proved.

2.2 Physical model

Referring to the bullet-shaped dry ice manufacturing mold proposed by Guevel[10], the physical model studied in this paper is shown in Fig. 1-a. The total computational domain size is 10 m×10 m×100 m. To ensure the grid size and quality around the inner wall surface and maintain computational accuracy, the mesh zone is divided into two parts based on the six-degree-of-freedom dynamic mesh, as shown in Fig. 1-b. The mesh in zone 1 is deformed or remeshed according to the results of the six degrees of freedom calculation, while the mesh in zone 2 moves together with the rigid body's movement without any change.

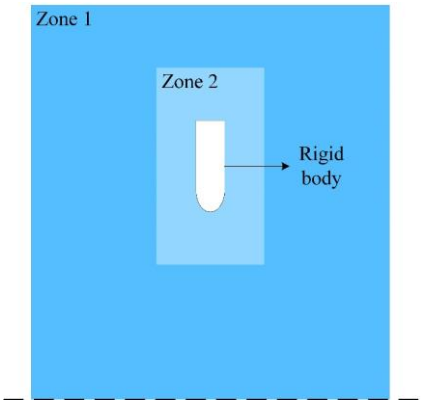

a. Mesh zone division

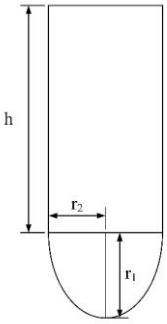

b. Physical model

Fig.1 Schematic of mesh zone division and the physical model

According to the shape of the settling body shown in Figure 1, parameters h, r_1, and r_2 are chosen to define the shape factors:

$$k_1 = \frac{r_1}{r_2}, k_1 = \frac{h}{r_2} \tag{6}$$

By changing the value of these two shape factors, the influence of shape on free settling is studied. The value of the two shape factors is shown in Table 2.

Table 2. Shape parameters

Item	Value
Density	1500 kg/m^3
Volume	1 m^3
Shape factor k_1	1,2,3,4
Shape factor k_2	1,2,3,4

3. RESULTS AND DISCUSSION

3.1 Surface pressure coefficient

The pressure distribution of fluid on the surface of a settling body results in pressure stresses on the surface, which contributes to the resistance in the direction of motion. Figure 2 shows the pressure contour plots of settling bodies with different shapes. The region with the highest pressure is located in the center of the front of the settling body. The pressure gradually decreases outward and exhibits a layered structure. As shape factor k_1 decreases, the maximum value of the pressure concentration zone in the center increases, but the area of the high-pressure zone significantly decreases overall. This indicates that the surface pressure stress distribution of the settling body with this shape is more concentrated in the central region, resulting in a reduction in the resistance caused by pressure stress generated by the fluid on the settling body.

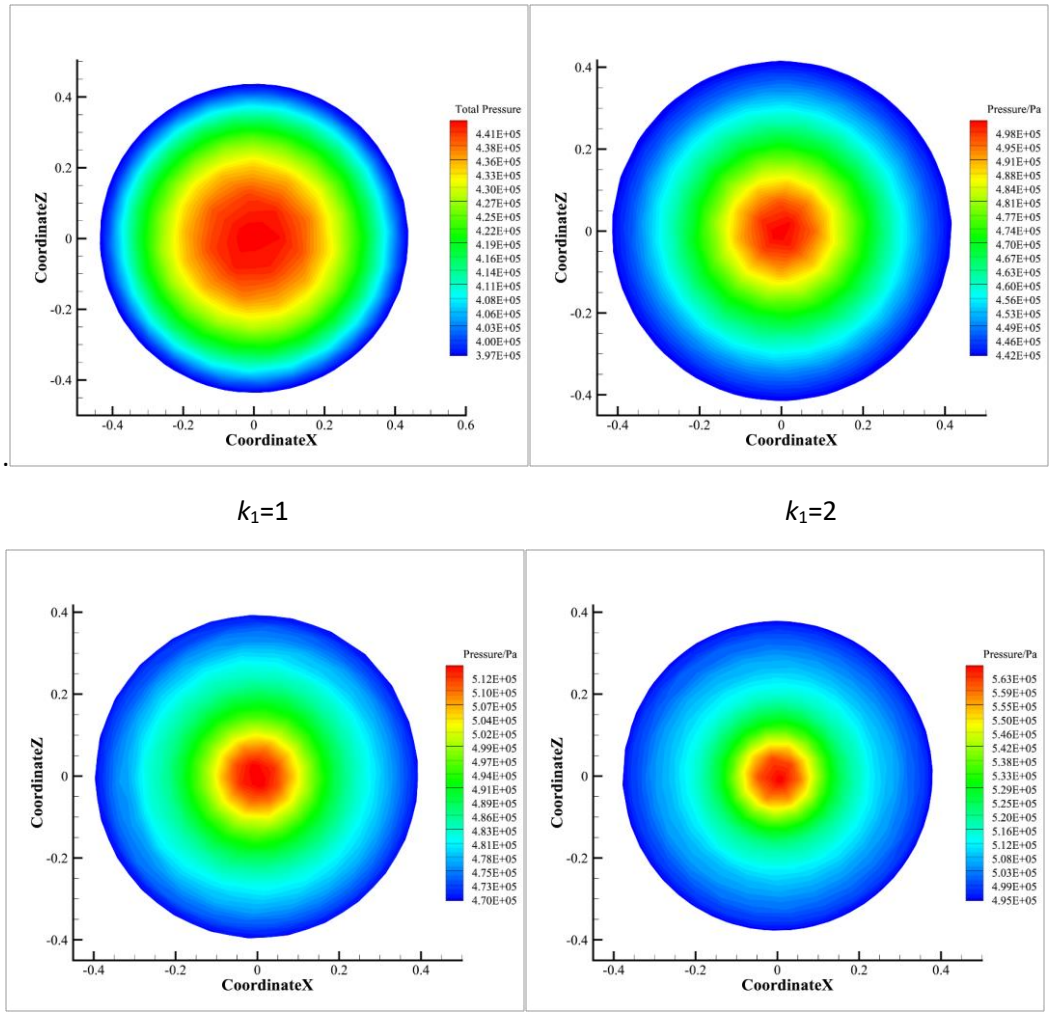

k_1=1 k_1=2

k_1=3 k_1=4

Fig.2 Contours of pressure distribution of settling bodies with different k_1

The pressure coefficient is a dimensionless number used to characterize the relative pressure in the flow field, defined as follows

$$C_{\mathrm{p}} = \frac{2P}{\rho_{\mathrm{f}} u^2} \tag{7}$$

Where C_{p} is the pressure coefficient, P is the difference between the static pressure at the calculation point and the independent static pressure away from any disturbance, ρ_{f} is the mass density of the fluid, u is the velocity.

As shown in Fig.3, under same shape factor k_2, the distribution of time-averaged surface pressure coefficient on the settling body with different shape factor k_1 can be compared. The results show that the distribution of time-averaged surface pressure coefficient under different shape factors is similar, with the maximum value at the front of the settling body and the minimum value at the rear end. As shape factor k_2 increases, the overall length of the settling body increases, and the difference between the maximum pressure coefficient value at the front and the minimum pressure coefficient value at the rear end also decreases, and so is the variation range of the pressure coefficient.

Furthermore, as shape factor k_2 increases, the surface pressure coefficient of the settling body with different shape factor k_1 decreases, but the relative difference in change is not significant. This is because the increase of shape factor k_2 improves the settling performance of the shapes with different shape factor k_1, and reduces the gap between them.

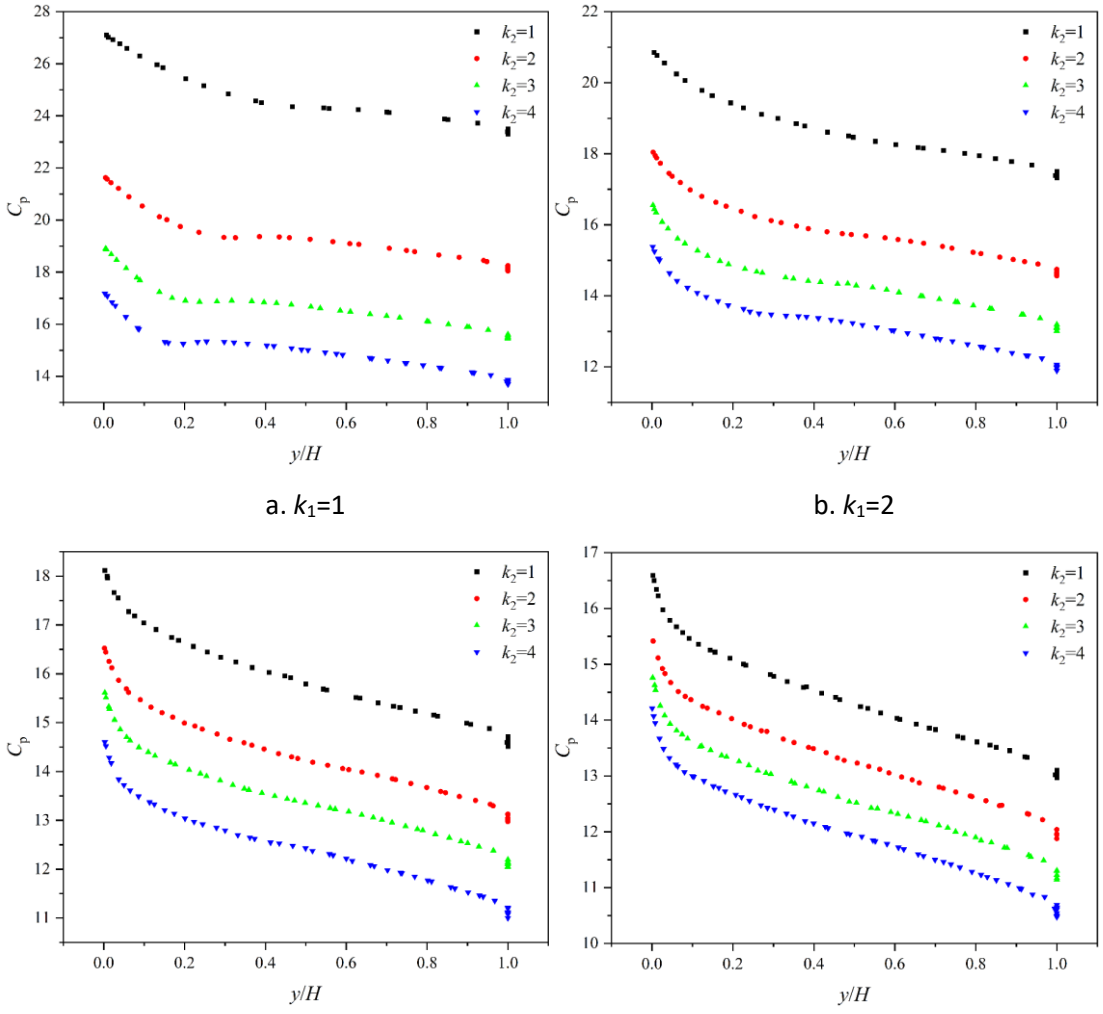

a. k_1=1 b. k_1=2

c. k_1=3 d. k_1=4

Fig.3 Comparison of surface pressure coefficients under the same k_1

3.2 Drag coefficient and settling velocity

During the settling process, the resistance the rigid body suffers is positively correlated with the velocity. As the settling velocity gradually increases, the resistance also increases. When the velocity increases to a certain value, the gravity, buoyancy, and resistance reach a

balance, that is, the free settling reached the terminal steady state.

$$\rho_s Vg - \rho_f Vg - F = 0 \tag{8}$$

The drag coefficient is a dimensionless treatment of the resistance, which is usually applied to the final equilibrium state. It tends to cause a larger coefficient in the development stage of settling, but it can still be used to divide different stages of settling development.

$$C_d = \frac{F}{qS} = \frac{2F}{\rho_f u^2 S} \tag{9}$$

Where F is the resistance, q is the dynamic pressure, S is the projected area, ρ_f is the mass density of the fluid, and u is the velocity.

The comparison of the drag coefficients in the terminal steady state of the settling body with different shape factors is shown in Fig.4. Under different *shape factor* k_2, with the increase of shape factor k_1, the final stable resistance coefficient of settlement decreases obviously, but with the increase of shape factor k_2, the degree of decline of the resistance coefficient decreases, and when shape factor k_1 is larger, the resistance coefficient of different shape factor k_2 settlement shapes The values are very close; for the same shape factor k_1, changing shape factor k_2 has little effect on the final stable resistance coefficient of settlement, only when k1 is small, there is a significant decrease, and when shape factor k_1 is large, shape factor k_2 has little effect on the terminal stable drag coefficient.

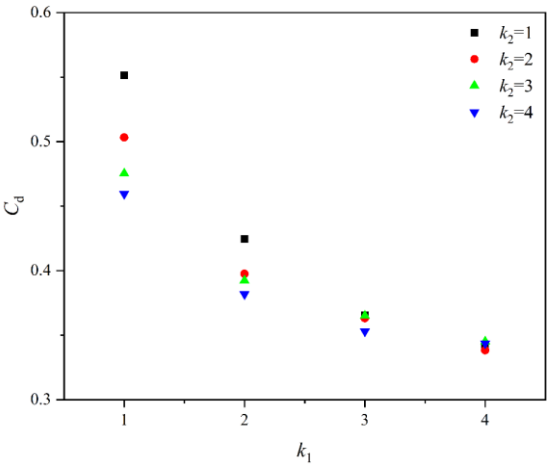

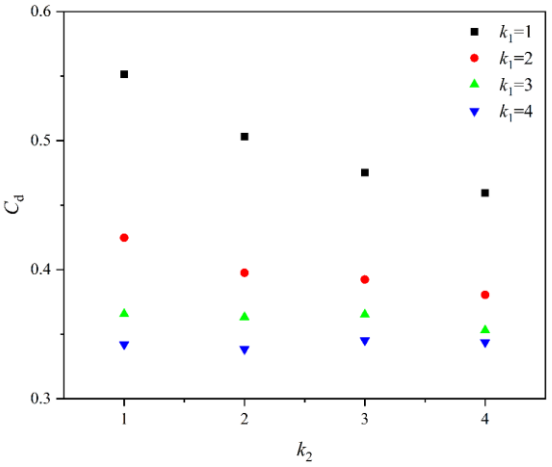

Fig.4 The terminal stable drag coefficient varies with k_1 and k_2

Fig.5 shows the contour of velocity distribution of the flow field near the settling body with different shape factors at the same time (t=7.5s), and the overall velocity distribution form is roughly the same. Comparing these figures, it can be observed that the fluid velocity field is larger in front of the settling body, which is the result of the fluid being influenced by the settling motion. As the value of shape factor k_1 at the front end of the settling body increases, the range of the fluid velocity field affected by the settling decreases. This is consistent with the changes in surface pressure distribution at the front end of the settling body mentioned in the previous section. It thus proves that larger values of shape factor k_1 result in smaller disturbances to the fluid in the vicinity of the settling body's head, resulting in lower resistance and a higher settling velocity.

The fluid from the upstream flow around the settling body and the boundary layer detachment from the side surface of the body forms a distinct wake flow field behind the body. The flow field shows significant velocity differentiation, with the maximum velocity in the core region of the wake flow gradually decreasing outward. Similarly, the size of the wake flow field is also related to the shape of the body. As the shape factor k_1 of the front end increases, the size of the wake flow field also decreases, especially the core region with higher velocity.

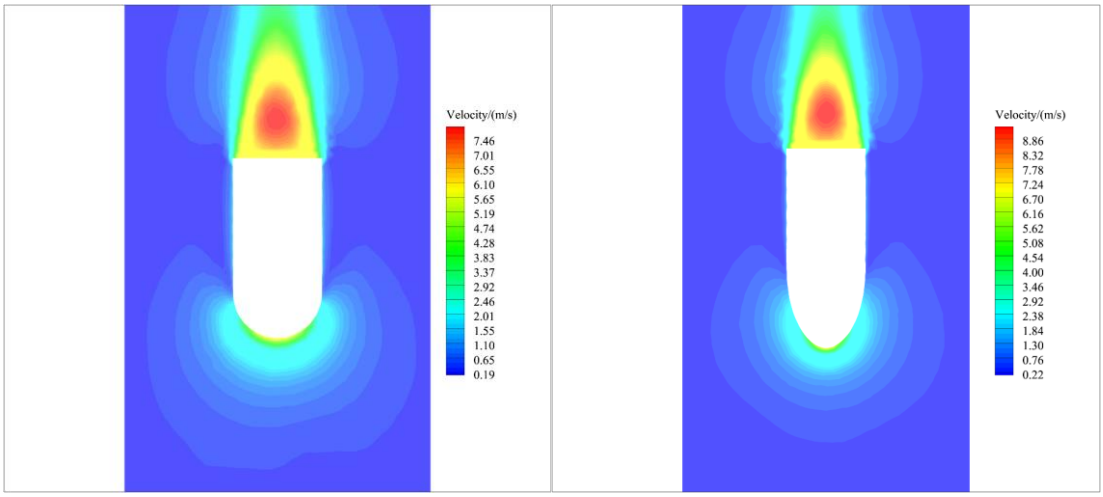

a. k_1=1 b. k_1=2

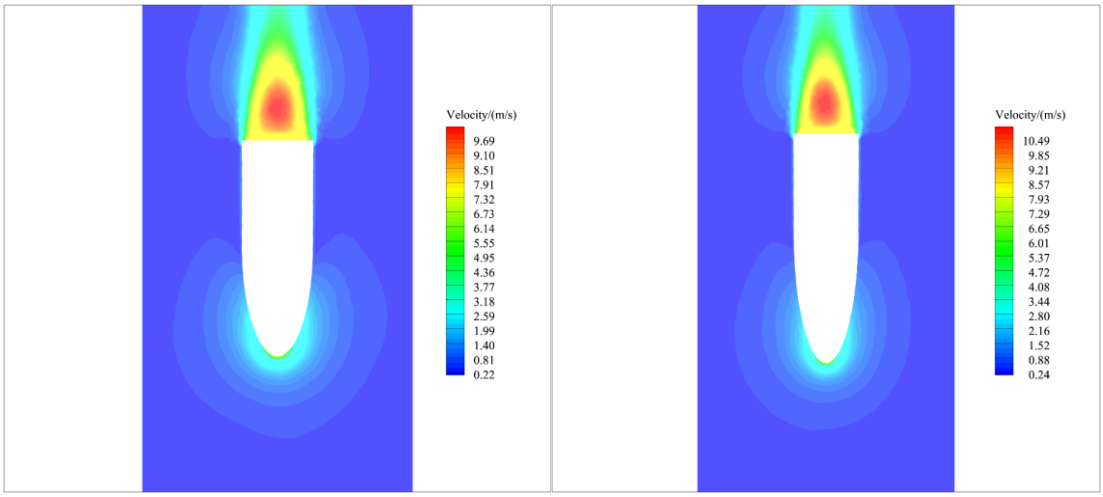

c. k_1=3 d. k_1=4

Fig.5 Contour of velocity distribution

The settling terminal velocities of different-shaped bodies are compared in Fig.6. With the increase of shape factors k_1 and k_2, the settling terminal velocities of the bodies increase. However, it is different for each shape: the growth rate of the settling terminal velocity slows down with the increase of shape factor k_1, while the settling terminal velocity shows an approximately linear relationship with shape factor k_2.

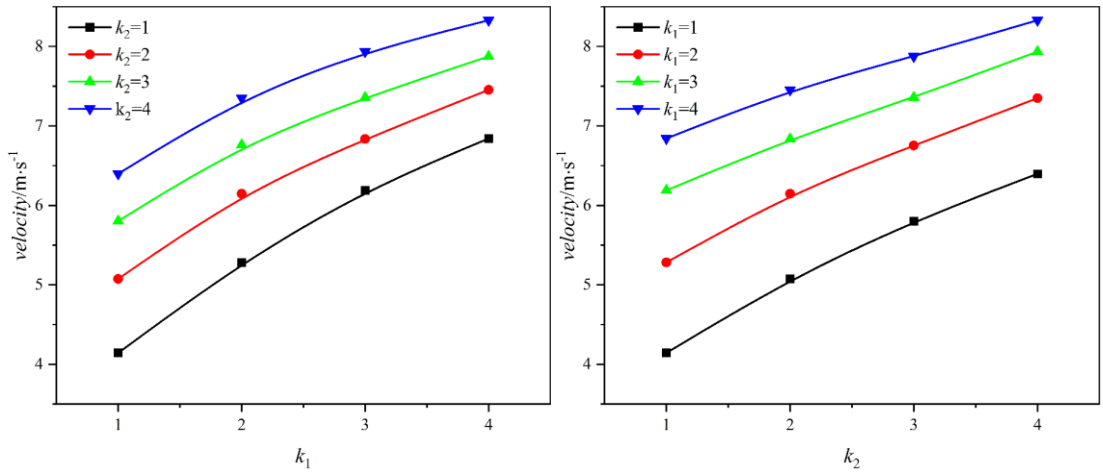

Fig.6 Terminal velocity varies with k_1 and k_2

3.3 Prediction of settling velocity

The Reynolds number is a dimensionless parameter used to characterize the flow condition of a fluid. Based on the Reynolds number, the fluid can be classified into different flow regimes, such as laminar flow and turbulent flow. The Reynolds number can also be used to determine the resistance experienced by an object in a fluid. It is described as

$$Re = \frac{\rho u l_c}{\mu} \tag{10}$$

Where ρ is the density of the fluid, u is the velocity, l_c is the characteristic length, and μ is the dynamic viscosity of the fluid.

When the settling body reaches the final stable state and the force satisfies Equation 2.2, the terminal velocity is described as:

$$u = \sqrt{\frac{2(\rho_s - \rho_f)Vg}{\rho_s S C_d}} \tag{11}$$

Combining the above equation with Re_t the Reynolds number of the terminal steady state, the equation can be obtained:

$$C_d Re_t^{\,2} = \frac{8\rho(\rho_f - \rho_s)Vg}{\pi\mu^2} \tag{12}$$

In the equation presented above, the right-hand side is not related to the settling terminal velocity. For a settling object with a fixed volume and density, the variable on the left-hand side of the equation is uniquely determined, and the Reynolds number of the terminal steady state only depends on the object's shape. Therefore, the aforementioned shape factors k_1 and k_2 are introduced, and Re_t the Reynolds number of the terminal steady state for objects of any shape can be related to these factors. The following form was found to be suitable for describing the relationship between Reynolds number and shape factors:

$$Re_t = Re_t(k_1, k_2) = \frac{a(a_1k_1 + a_2k_2 + a_3k_1k_2 + c)}{(b_1k_1 + b_2k_2)^d} \tag{13}$$

The expression of the shape factors to the Reynolds number of the terminal steady state can be obtained by fitting the numerical simulation data, and the error range between the predicted Reynolds number and the numerical simulation Reynolds number is within ±2.5%. Based on the above formula, it is possible to predict the settling terminal velocity of objects with similar shapes within a certain range, for any settling body with a certain volume.

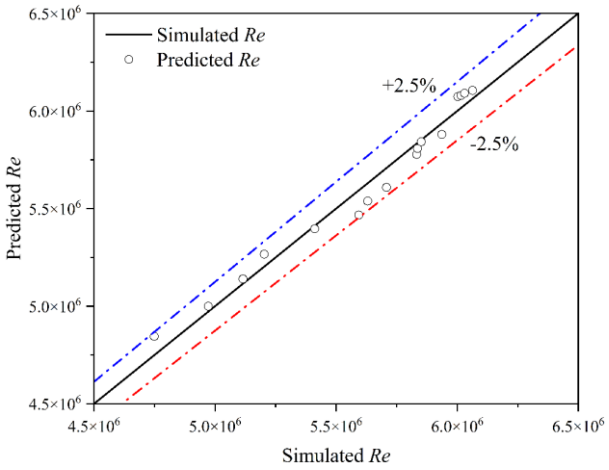

Fig. Comparison of predicted *Re* and simulated *Re*

4. CONCLUSION

The six DOF dynamic mesh and CFD methods are employed to conduct numerical simulations of the free settling of large streamlined objects. Dimensionless shape factors are extracted and used to analyze the dynamic behavior of settling bodies with different shape factors during the settling process. The study also investigates the impact of shape factors on settling performance. The main conclusions include:

(1) The settling performance of shapes with different shape factors was analyzed based on the surface pressure coefficient, terminal drag coefficient, and settling velocity. As the shape factors k_1 and k_2 increase, the pressure coefficient and terminal drag coefficient decrease, while the settling velocity increases accordingly.

(2) Based on the numerical simulation results, a formula for predicting the terminal settling velocity of objects based on the shape factors has been derived. This formula can serve as a valuable reference for the design of dry ice shapes in dry ice throwing, thereby enabling more efficient ocean carbon sequestration.

DECLARATION OF INTEREST STATEMENT

The authors declare that they have no known competing financial interests or personal relationships that could have appeared to influence the work reported in this

paper. All authors read and approved the final manuscript.

REFERENCE

[1] China Ship Survey. CCUS, explosive force of thi ck product [R/OL]. (2022-09) [2022-07-01]. http s://mp.weixin.qq.com/s/NNe01leZDCW7ve fvXnnc Jg.

[2] LTD. PS E. DNV and PSE Report on Ship CarbonCapture & Storage[J]. Business Wire (English),2013.

[3] The Naval Architect. Cryogenic technology project keeps its cool over carbon targets [R/OL]. (2020-03) [2022-07-01]. https://www.rina.org.uk/Cryogenic_technology_pr oject_keeps_its_cool_over_carbon_targets.html.

[4] K line will launch the world's first ship capable of capturing CO2[J]. Marine Electric & Electronic Technology, 2020, 40 (10): Front insert 10. (in Chinese)

[5] GABITTO J, TSOURIS C. Drag coefficient and settling velocity for particles of cylindrical shape [J]. Powder Technology, 2008, 183(2): 314-22.

[6] DIOGUARDI F, MELE D. A new shape dependent drag correlation formula for non-spherical rough particles. Experiments and results [J]. Powder Technology, 2015, 277: 222-30.

[7] LI Y, YU Q, GAO S, et al. Settling velocity and drag coefficient of platy shell fragments [J]. Sedimentology, 2020, 67(4): 2095-110.

[8] XIANG G, GUEDES SOARES C. Improved dynamical modelling of freely falling underwater cylinder based on CFD [J]. Ocean Engineering, 2020, 211.

[9] Nakashiki, N, Ohsumi, T, and Shitashima, K. Sequestering of CO sub 2 in a deep-ocean - fall velocity and dissolution rate of solid CO sub 2 in the ocean. Japan: N. p., 1991. Web.

[10] GUEVEL P, FRUMAN D H, MURRARY N.Conceptual design of an integrated solid CO2 penetrator marine disposal system[J]. Energy Conversion and Management, 1996, 37(6):10531060.

[11] CHENG N-S. Comparison of formulas for drag coefficient and settling velocity of spherical particles [J]. Powder Technology, 2009, 189(3): 395-8.